

Curvature maser emission due to field line torsion in pulsar magnetospheres

Qinghuan Luo and D. B. Melrose

Research Centre for Theoretical Astrophysics, School of Physics, University of Sydney, NSW 2006, Australia

Accepted 1995 March 24. Received 1994 October 14; in original form 1994 April 25

ABSTRACT

Field line geometric effects on curvature emission and absorption are explored in detail. In particular, we consider field line distortion near the star's surface due to a quadrupolar component, with the field line geometry approximated by a local helix. The spectral power for a particle moving along the field line is derived from the familiar synchrotron formula, and the absorption coefficient is derived by appealing to the Einstein coefficients. Field line torsion can result in wave amplification, with the maser emission occurring very nearly along the field lines. The maser emission can be saturated by quasi-linear diffusion. The application of such maser emission to pulsar radio emission is discussed.

Key words: masers – plasmas – radiation mechanisms: nonthermal – stars: magnetic fields – pulsars: general.

1 INTRODUCTION

In earlier investigations of curvature emission and absorption, the magnetic field lines were assumed to be locally circular (Luo & Melrose 1992, and references cited therein). This is a reasonable assumption provided that the field lines are confined to a plane. There are at least two regions in a pulsar magnetosphere where this assumption may not be satisfied: the region near the stellar surface where high-order multipoles may be important (Ruderman & Sutherland 1975; Blandford 1975; Ruderman 1991; Krolik 1991) and the region near the light cylinder where the field lines are swept back as a result of rotation (Blandford 1975; Shitov 1983). We refer to any non-dipole geometry that involves the magnetic field lines deviating out of a plane as a 'torsion' (cf. Section 2). A field line with torsion has two radii of curvature in orthogonal planes. One example is a twisted field line; cf. equation (8).

An important consequence of the inclusion of field line torsion in curvature emission is that it can give rise to maser emission (Luo 1993). This mechanism for maser emission is complementary to that due to curvature drift (Luo & Melrose 1992). As shown previously (Luo 1993), maser emission due to field line torsion may be attributed to an asymmetry in the radiation pattern about the particle orbit (in this case it is along field lines). In the presence of field line torsion, a particle trajectory not only curves in its osculating plane (which coincides with the field line osculating plane when the curvature drift is neglected) but also curves out of

this plane. As a consequence, the beam pattern of the radiation is asymmetric about the particle orbit. This asymmetry in the beam pattern can result in maser emission in the same way as the curvature drift allows maser emission by introducing an asymmetry into the emission pattern.

The purpose of this paper is to explore this mechanism further in application to pulsar radio emission. We consider only the simplest geometry of the field lines with torsion: a locally helical field line. In such a geometry, the curvature and torsion radii are locally constant. The spectral power for a particle moving along a helical orbit is well understood, as it corresponds to the case of synchrotron emission by a particle spiralling around a magnetic field line. The absorption coefficient is determined from the spectral power by appealing to the Einstein coefficients (e.g. Melrose 1980).

In the application to pulsars, we consider a model in which the non-dipole field is attributed to a quadrupole near the star's surface. This non-dipole field line configuration was also used by Barnard & Arons (1982) in constructing a polar cap model for non-dipole fields. Field line twisting occurs when the dipole and quadrupole axes are not aligned. Because of the quadrupole, the usual axisymmetry is broken. The field line structure in one polar cap region is different from that in the other. Near one pole (of the dipole) the dipole and quadrupole fields have the same polarity and complement each other, giving rise to field lines tipped towards the quadrupole axis, compared with a purely dipole field. Near the other pole the dipole and quadrupole components have opposite polarity, weakening the field near the

star; the cone of open dipole field lines at large distances splits into two cones near the stellar surface (cf. Kuz'min 1992).

In Section 2, we introduce the wave transfer theory needed to study absorption of waves in the medium. The spectral power for a particle moving along a locally helical field line is derived by analogy with the corresponding synchrotron formula. In Section 3, torsion-induced maser emission is discussed and compared with the curvature-drift mechanism. In Section 4, the theory of maser emission due to torsion is applied to pulsar radio emission. Saturation of maser emission is briefly discussed in Section 5.

2 CURVATURE MASER EMISSION DUE TO TORSION

2.1 Wave transfer equation

The absorption of waves propagating through a medium is described by a wave transfer equation (e.g. Chandrasekhar 1960, p. 9). The level of the radiation is conveniently described by the specific intensity, $I(\mathbf{k}, s)$, which is defined as the energy per unit solid angle through unit area normal to the displacement s along the ray path. Generally, in an anisotropic medium the ray direction is different from the wave-normal direction, defined by the wave vector \mathbf{k} . The continuous bending or refraction of a ray due to this anisotropy may be important in the context of polarization properties of pulsar radiation; for detailed discussion, see, e.g., Melrose (1979) and Barnard & Arons (1986). However, the difference between the wave normal and the ray direction is neglected here. The medium is also assumed locally homogeneous so that the dependence on s is suppressed in the following discussion. Let $\alpha(\mathbf{k})$ be the (spontaneous) power radiated per unit volume in \mathbf{k} -space (e.g. Rybicki 1984) and let μ be the absorption coefficient per unit length in s . One defines the optical depth and the source function by writing

$$\tau = \int_{s_0}^s \mu \, ds, \quad (1)$$

and

$$S = \frac{1}{\mu} \alpha(\mathbf{k}), \quad (2)$$

respectively. The wave transfer equation can be integrated to yield

$$I = I_0 e^{-\tau} + \int_0^\tau d\tau' e^{-\tau'} S(\tau'), \quad (3)$$

where I_0 is the specific intensity of the incident radiation. In equation (3), $S(\tau)$ is obtained by expressing (2) in terms of the optical depth $\tau(s)$. One may define the absorption coefficient per unit time, Γ , by

$$\mu = \frac{\Gamma}{v_g}, \quad (4)$$

where v_g is the group speed. In the following discussion we assume $v_g \approx c$ and that the absorption coefficient Γ can be

derived using the Einstein coefficients. Wave amplification (or maser emission) corresponds to an optical depth (2) that is negative, $\tau < 0$.

An observationally relevant quantity is the radiation flux density $F(\mathbf{k})$, which is obtained by integrating the specific intensity over the solid angle about \mathbf{k} . Consider a source whose characteristic dimension is much less than the distance to the observer, as in the case of pulsar emission. Then, from (3), one has the radiation flux density

$$F(\mathbf{k}) = \frac{1}{D^2} \int_{V_s} dV \alpha(\mathbf{k}) \exp[-\tau(\mathbf{k})], \quad (5)$$

where V_s is the source volume of the radiation, and D is the distance between the source and observer. For present purposes, $I_0 = 0$ is assumed. Then, to account for the observed flux level, the optical depth in equation (5) must satisfy $\tau \ll -1$.

The absorption coefficient in equation (4) can be written down by using the Einstein coefficients (e.g. Melrose 1980). In doing so, the following one-dimensional approximation to the particle motion is made. In a pulsar magnetosphere, the particle motion can be separated into perpendicular and parallel parts (in reference to the magnetic field line), with the perpendicular motion quantized into discrete energy levels (called Landau levels). The time-scale for a particle to lose all its perpendicular energy to synchrotron radiation and fall to the lowest Landau level is

$$t_s \approx 3.47 \times 10^{-14} (\gamma/10^2) / (B/10^8 T)^2 \text{ s},$$

where γ and B are the Lorentz factor and the magnetic field, respectively. Due to the strong magnetic field, this time-scale is so small that all the particles should be in their lowest Landau levels. Therefore the particle motion in a pulsar magnetosphere (well within the light cylinder) is essentially one-dimensional.

In the one-dimensional approximation, using the Einstein coefficients, the absorption coefficient Γ can be written as (cf. Melrose 1978)

$$\Gamma(\omega, \mathbf{k}) = -\frac{(2\pi c)^3 N_0}{\omega^2 m c^2} \int_0^\infty d\gamma \frac{df(\gamma)}{d\gamma} \eta(\omega, \theta, \gamma), \quad (6)$$

with $\hat{\mathbf{k}} = \mathbf{k}/k$, and where $\eta(\omega, \theta, \gamma)$ is the spectral power of a single particle, N_0 is the particle density, γ is the Lorentz factor of the parallel motion and $f(\gamma)$ is the particle distribution function normalized to unity. For maser emission to occur there must be some domain in γ over which both the following conditions apply:

$$df(\gamma)/d\gamma > 0, \quad (7a)$$

$$d\eta/d\gamma < 0. \quad (7b)$$

The condition (7a) is obvious from (6) since η is always positive. This condition requires an effective particle population inversion which provides free energy to sustain the maser emission. The second condition is obtained by a partial integration of (6).

2.2 Locally helical field lines

Evaluation of the absorption coefficient (6) involves calculation of the spectral power associated with a particle moving

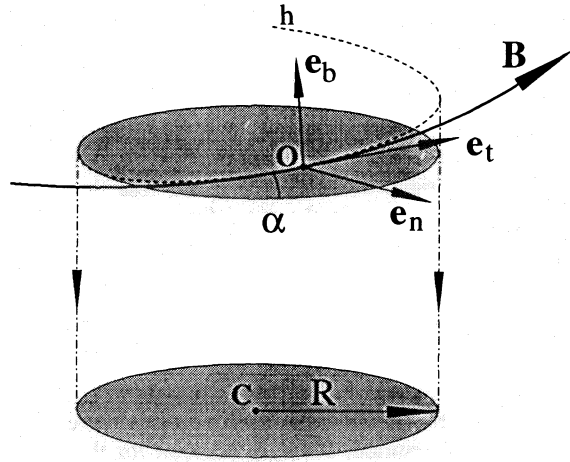


Figure 1. A locally helical field line. The magnetic field line through a point ‘O’ is locally indistinguishable from a helical curve h . The ‘pitch angle’ is $\pi/2 - \alpha$ and the radius of the projected circle is R . The field line tangent, normal and binormal are e_t , e_n and e_b , respectively. They satisfy $e_b = e_n \times e_t$.

along the field line. Here we consider the case where the field line is twisted, described by a curvature radius and a torsion radius. For a planar field line the curvature radius is defined as the radius of the circle that lies in the field line plane and has maximum fit (contact) with the field line. The curvature radius of a twisted field line can be defined in a way similar to the planar case; i.e. it is defined as the radius of the circle that lies in the osculating plane (the plane defined by the tangential and normal directions of the field line) and this circle has maximum contact with the field line. At different points along the field line the normal directions of each osculating plane (called the binormals) are not parallel. The rate of change of the binormal with respect to the position is called the torsion, and the modulus of its reciprocal is called the torsion radius. Due to the beaming effect of radiation by ultrarelativistic particles, one can assume that the dimension of the emission region is much smaller than the curvature and torsion radii. Thus the twisted field lines can be approximated locally by a helical curve (Fig. 1).

As shown in Fig. 1, for a locally helical curve, both torsion and curvature radii are locally constant. For convenience of calculation, we define the angle, α , such that the ‘pitch angle’ is $\pi/2 - \alpha$ (cf. Fig. 1). We also define a plane on to which the projection of the field line is locally a circle with a radius R . The curvature radius and torsion radius are now given by

$$R_B = R(1 + \tan^2 \alpha), \quad (8)$$

$$R_\tau = \frac{R}{|\tan \alpha|} (1 + \tan^2 \alpha), \text{ with } |\alpha| < \frac{\pi}{2},$$

respectively. Negative α is allowed and corresponds to twisting in the opposite direction (positive torsion, by definition, corresponds to field lines curving out of its plane in the binormal direction). For small α , one has $R_B/R_\tau \approx |\tan \alpha| \approx |\alpha|$. Thus $|\alpha|$ can be interpreted as the ratio of the curvature radius to the torsion radius. A locally circular field line corresponds to the special case, $\alpha = 0$ and hence $R_\tau = \infty$, $R_B = R$.

2.3 Spectral power

To calculate the spectral power, one needs to write down an explicit expression for the polarization of the relevant waves. In a pulsar magnetosphere, the length-scale characterizing inhomogeneity due to the curvature and the torsion of field lines is R_B (when $R_B < R_\tau$), which is much larger than the interaction length-scale characterized by $\Delta\theta_0 R_B$, where $\Delta\theta_0$ is the angular spread of the radiation pattern and where R_B and R_τ are the curvature and torsion radii, respectively (cf. Section 2.2). Thus in writing down the polarization, the field line is treated as locally uniform. In this approximation, the possible waves are in the ordinary and extraordinary modes (e.g. Arons & Barnard 1986). In the following discussion we consider only transverse (or quasi-transverse) waves with frequency in the radio range. In close analogy to the magnetoionic theory, the polarization vector for quasi-transverse waves can be written approximately as

$$e = \frac{L\hat{k} + T\hat{t} + i\hat{a}}{(1 + T^2)^{1/2}} \approx \frac{T\hat{t} + i\hat{a}}{(1 + T^2)^{1/2}}, \quad (9)$$

where T and L are the transverse and longitudinal polarization coefficients which in general depend on θ . The approximation in equation (9) is valid for $|L| \ll |T|$. The unit vectors \hat{k} , \hat{t} and \hat{a} form an orthonormal set:

$$\hat{k} = k/k, \quad (10a)$$

$$\hat{a} = \mathbf{B} \times \hat{k}, \quad (10b)$$

$$\hat{t} = (\mathbf{B} \times \hat{k}) \times \hat{k}, \quad (10c)$$

with $\mathbf{B} = \mathbf{B}/B$. For pulsars, due to the strong magnetic field, one has $\omega_B/\omega \gg 1$ (where ω_B is the non-relativistic gyrofrequency), and in the small angle approximation, $|\theta| \ll 1$, the polarization coefficients reduce to $T \approx 0$ for the x-mode and $T \approx \infty$ for the low-frequency branch of the o-mode provided that the electron–positron plasma is quasi-neutral (Arons & Barnard 1986; Lominadze et al. 1986).

In the calculation of the spectral power, traditionally, emission is treated by evaluating the Poynting vector from the fields generated by a source, e.g. an accelerated motion of a particle (Jackson 1968). The spectral power is found by calculating the power crossing an arbitrary sphere enclosing the source. In the presence of a medium, it is more convenient to derive the spectral power by considering the rate per unit volume at which work is done by a current (associated with the source) on the field that it generates (Melrose 1980). A derivation of the synchrotron spectral power by this method is outlined in Melrose (1980). The curvature spectral power including field line torsion can be obtained through the synchrotron formula (A1), since the field line is locally indistinguishable from the helical curve (see Fig. 1).

Let \mathbf{k} be through the point ‘O’ and let it be at an angle θ to the osculating plane of the field line \mathbf{B} . For quasi-transverse waves, assuming that the Lorentz factor is well below the threshold ($\gamma \sim 10^3$) above which the curvature drift is important (cf. Sections 3 and 4.1), the curvature spectral power is given by [see equation (A1) in Appendix A]

$$\eta(\omega, \theta) = \frac{q^2 \omega^2}{24\pi^4 \epsilon_0 c \omega_R (1 + T^2)} \times \left| \sigma T \xi^{-1} K_{1/3}(y) + n\beta \cos \alpha \xi^{-2} K_{2/3}(y) \right|^2, \quad (11)$$

where

$$\beta = \frac{v}{c}, \quad (12a)$$

$$\sigma = \frac{\sin(\alpha + \theta) - n\beta \sin \alpha}{\cos(\alpha + \theta)}, \quad (12b)$$

$$\xi = \left[\frac{n\beta \cos \alpha \cos(\alpha + \theta)}{2(1 - n\beta \cos \theta)} \right]^{1/2}, \quad (12c)$$

$$y = \frac{\omega}{2\omega_R} n \cos \alpha \cos(\alpha + \theta) \xi^{-3}, \quad (12d)$$

$$\omega_R = \frac{c}{R} \cos \alpha, \quad (12e)$$

and where n is the refractive index. In deriving (11), we assume that the refractive index satisfies the condition $|n - 1| \ll 1$ such that $1 - n\beta \cos \theta > 0$. This condition is trivially satisfied by the extraordinary mode with $n = 1$. Now we show that the low-frequency branch of the ordinary mode (o-mode) can also satisfy this condition provided that waves propagate at a sufficiently small angle to the magnetic field line with $\omega/\omega_p \ll 1$, where ω_p is the non-relativistic plasma frequency.

For the low-frequency branch of the o-mode with polarization perpendicular to the field line plane, the dispersion relation is (Arons & Barnard 1986; Luo, Melrose & Machabeli 1993)

$$\omega^2 = k_\phi^2 c^2 \left(1 - \frac{k_z^2 c^2}{8\langle \gamma \rangle \omega_p^2} \right), \quad (13)$$

where k_ϕ and k_z are the components of \mathbf{k} along and binormal to \mathbf{B} , respectively, and where $\langle \gamma \rangle$ is the average Lorentz factor of the plasma. For a dense plasma ($\omega/\omega_p \ll 1$), equation (13) describes waves with polarization perpendicular to the field line plane, i.e. the polarization is given by equation (9) with $T = \infty$. The approximation in (9) is appropriate, as the dense plasma shorts out the parallel electric field of waves. The dispersion relation (13) implies

$$1 - n \approx -n^2(\theta^2 + \delta)/2, \quad (14)$$

with $\delta = k_z^2 c^2 / (8\langle \gamma \rangle \omega_p^2)$ and where the approximation $\cos \theta \approx 1 - \theta^2/2$ is made. Thus the condition that the refractive index be close to unity (dispersion can be neglected) implies that both the dispersion correction δ and the propagation angle θ be sufficiently small. Since

$$1 - n\beta \cos \theta = 1 - n + n(1/\gamma^2 + \theta^2)/2, \quad (15)$$

the condition $1 - n\beta \cos \theta > 0$ implies that $\delta < 1/\gamma^2$.

2.4 Maser emission

Maser emission corresponds to the absorption coefficient (6) being negative for a certain range of parameters (e.g. within a certain angular range). Using equations (6) and (11) one obtains the absorption coefficient for the o-mode:

$$\Gamma_o = \frac{2}{3} \left(\frac{\omega_p^2}{\omega_R} \right) \int d\gamma f(\gamma) \sigma \xi^{-2} \gamma^{-3} K_{1/3}(y) \times \left[-\frac{n\beta \sin \alpha}{\cos(\alpha + \theta)} K_{1/3}(y) + \frac{3\sigma y}{2(1 - n\beta \cos \theta)} K_{2/3}(y) \right]. \quad (16)$$

In deriving (16) we use $T = \infty$ and the term $\propto K_{2/3}(y)$ in (11) can be dropped. The presence of the first term in the square brackets is due to the fact that $d\sigma/d\gamma \neq 0$ for $\alpha \neq 0$. For $\alpha = 0$, the absorption coefficient reduces to that for curvature emission in the absence of both torsion and curvature drift, in which case the absorption coefficient is always positive (since the first term in the square brackets vanishes). For $\alpha \neq 0$ the absorption coefficient (16) can be negative for some range of θ since the coefficient of the term $[K_{1/3}(y)]^2$ in equation (16) can be negative.

The factor σ in equation (11) plays a crucial role in the resulting negative absorption. With the small-angle approximation we have

$$\sigma \approx \theta + \alpha/2\gamma^2. \quad (17)$$

Compared with the planar field line case, there is an angular shift $\alpha/2\gamma^2$, which is a shift in the peak of the single-particle emission spectrum away from $\theta = 0$. This shift is dependent on the particle energy as well as on the torsion. This angular shift plays essentially the same role as the curvature drift in Luo & Melrose (1992), except that it does not depend on the sign of the charge. However, this angular shift depends explicitly on the sign of α , i.e. the direction of field line twisting. As the particle energy changes (as a result of the emission of a photon) the centre of the energy spectrum shifts in the parallel or antiparallel direction with respect to the binormal of the magnetic field lines. Due to the energy-dependent angular shift in (11), the condition (7b) can be satisfied and maser emission can occur.

Figs 2 and 3 show plots of the normalized absorption coefficient $\Gamma/(\gamma\omega_R)$ versus θ for different Lorentz factors (in the case of a monoenergetic distribution). All negative absorption profiles are single-peaked and narrow. The amplification occurs approximately in the field line direction. When the frequency is $\omega \sim \gamma^3\omega_R$, the curves represent optical depth versus viewing angle. For illustrative purposes, the parameters are chosen as $\alpha = 0.1$ (cf. Section 4.2), the frequency $\omega = 10^8 \text{ s}^{-1}$, $R_B = 1.5 \times 10^5 \text{ m}$, and the particle density $N_0 = 5 \times 10^{21} \text{ m}^{-3}$. With these parameters we have $\delta \leq 10^{-18}$. Since the angular range within which the amplification occurs is about 10^{-4} , from equation (14) we have $|1 - n| \approx 10^{-8}$, and hence the dispersion effect is not important. Thus the approximation $n \approx 1$ is appropriate.

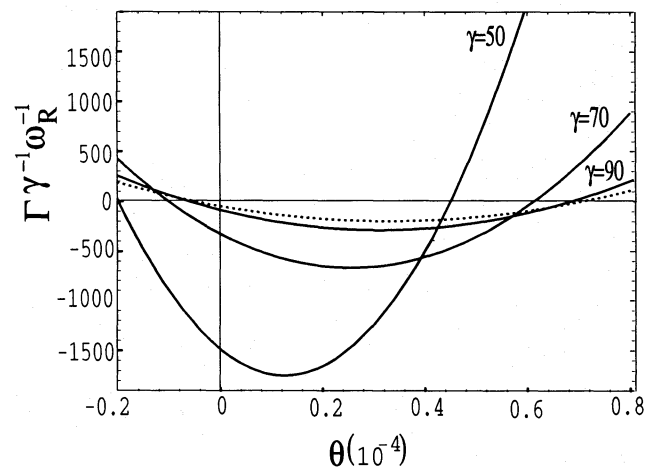


Figure 2. Normalized absorption coefficient is plotted as a function of θ , with θ in rad. The dotted curve corresponds to $\gamma = 100$.

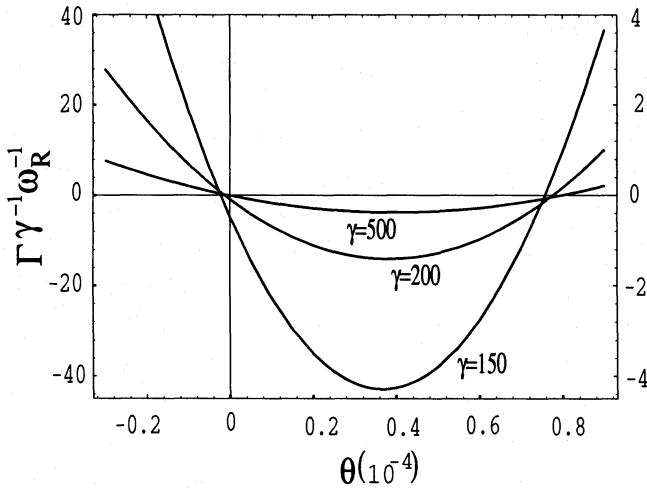


Figure 3. Normalized absorption coefficient versus θ , with θ in rad. The vertical scale on the right-hand side is for the curve $\gamma=500$.

One can show that maser emission is not possible for the extraordinary mode (x-mode) waves. Analogous to (16), for the x-mode we have

$$\Gamma_x = \frac{2}{3} \left(\frac{\omega_p^2}{\omega_R} \right) \int d\gamma f(\gamma) \cos^2 \alpha \xi^{-4} \gamma^{-3} K_{2/3}(y) \times \left[K_{2/3}(y) + \frac{3y}{2(1-\beta \cos \theta)} K_{1/3}(y) \right], \quad (18)$$

which is essentially the same as that for the planar field line case except for a factor $\cos^2 \alpha$. Thus the absorption coefficient is always positive.

3 COMPARISON WITH CURVATURE-DRIFT-INDUCED MASER EMISSION

The maser emission discussed here is similar to the curvature drift mechanism (Luo & Melrose 1992) in that, for both curvature-drift-induced maser emission (CDIME) and torsion-induced maser emission (TIME), (i) the maser action relies on the spectral asymmetry due to the dependence of the angular shift on γ ; (ii) maser emission occurs only in a limited angular range; and (iii) the Lorentz factor must exceed a threshold.

For CDIME, the angular shift is introduced through the curvature drift angle $\theta_d = v\gamma/(\omega_B R_B)$ which is proportional to the particle energy $mc^2\gamma$ (Luo & Melrose 1992). The curvature drift shifts the peak of the angular distribution of radiation from $\theta=0$ to $\theta=\theta_d$, so that $d\eta/d\gamma$ contains a term $-(\partial\eta/\partial\theta)d\theta_d/d\gamma$, which can lead to negative Γ when the particle energy is sufficiently high. Similar to CDIME, the angular shift in TIME is introduced via equation (17) which is also dependent on the particle energy. Thus the TIME mechanism can be interpreted essentially in the same way as for CDIME.

Both CDIME and TIME require that the Lorentz factor exceed a threshold. For CDIME, this minimum is $\gamma \sim 10^3$ to 10^4 (Luo & Melrose 1992) and is derived from the condition $\gamma^2 \theta_d \Delta \theta_0 > 1$, with $\Delta \theta_0$ being the largest possible angular

range. The minimum Lorentz factor for TIME can be derived by comparison of the first term with the second term in equation (16), since negative absorption is possible only when the first term is larger than the second in magnitude. The estimated minimum Lorentz factor is much less than that for CDIME. A detailed discussion is given in Section 4.1.

Despite the similarities between these two mechanisms, there are important differences.

(a) TIME always occurs nearly along the field line direction at $\theta_0 \approx (1/6)(3\omega_R/\omega)^{2/3}\alpha$ (Luo 1993). This contrasts with CDIME, where the amplification occurs at $\theta_0 \approx \Delta \theta_0 = (3\omega_R/\omega)^{1/3} \gg |\theta_d|$ (Luo & Melrose 1992), which is larger than that for TIME. For TIME, if θ were too large it would dominate over the angular shift $\alpha/2\gamma^2$, leading to net absorption ($\sigma \approx 0$).

(b) In CDIME, the drift angle is $\propto \gamma$, and a larger γ gives rise to a larger drift angle θ_d . Hence CDIME occurs at large γ . In contrast, TIME occurs for a relatively small Lorentz factor since the angular shift is $\propto 1/\gamma^2$ [cf. equation (17)] and a smaller γ gives rise to a larger angular shift.

(c) Unlike CDIME, TIME is not sensitive to the magnetic field strength. However, there is an overall constraint on the magnetic field strength due to the one-dimensional condition, which requires that the magnetic energy density be much larger than the particle energy density (cf. equation 6). This constraint can be easily satisfied for a pulsar magnetosphere.

(d) The angular shift in equation (17) depends explicitly on the ratio of the curvature radius to the torsion radius (here negative α is allowed), but it is insensitive to the sign of the charge. For CDIME, the angular shift θ_d depends explicitly on the particle charge ($\theta \propto 1/\omega_B$). Thus, unlike CDIME, in which electrons and positrons give opposing contributions to Γ , TIME applies to a quasi-neutral plasma with electrons and positrons giving contributions with the same sign to Γ .

There is a close analogy between curvature emission and synchrotron emission, with, in practice, one notable difference being that curvature emission applies to a one-dimensional distribution and synchrotron emission applies to a three-dimensional distribution. In the simplest cases neither can lead to maser emission. Maser synchrotron emission is possible when either (i) the effect of the ambient plasma is taken into account (McCray 1966; Zheleznyakov 1967), or (ii) the pitch-angle distribution is sufficiently anisotropic (Zheleznyakov & Suvorov 1972). The effect of the ambient medium applies for an isotropic distribution of particles, and is due to the emissivity being modified in such a way [essentially a replacement $\gamma \rightarrow \gamma(1 + \gamma^2 \omega_p^2/\omega^2)^{-1/2}$ in relevant terms] that $\partial\eta/\partial\gamma$ can be negative (for $\gamma\omega_p \sim \omega$). In contrast, maser curvature emission is due to a (γ -dependent) modification of the angular dependence of the emission, so that $(\partial\eta/\partial\theta)(d\theta/d\gamma)$ can be negative, where the angular deviation, $\Delta\theta$, is different for TIME and CDIME.

4 PULSAR RADIO EMISSION

In the foregoing discussion we show that particles moving along twisted field lines can amplify waves with electric field approximately in the binormal direction of the field line osculating plane. In this section we consider the application

to pulsar radio emission and in particular we show that this mechanism may produce the observed radio pulses provided that certain conditions are satisfied.

4.1 Conditions for maser emission

The threshold condition on γ for growth is derived as follows. In equation (16), the term $\propto yK_{1/3}(y)K_{2/3}(y)$ is always positive. From equation (12d) we have $y \propto 1/\gamma^3$. Negative absorption requires that this term be smaller than the term that is proportional to $[K_{1/3}(y)]^2$. This in turn implies that the Lorentz factor must satisfy (Luo 1993)

$$\gamma \gtrsim \left(\frac{\omega}{\omega_R} \right)^{1/3}, \quad (19)$$

where $\omega_R \approx c/R_B$. For parameters used in Figs 2 and 3, the minimum Lorentz factor required for maser emission is $\gamma \approx 37$, which is much smaller than required for CDIME [$\gamma > (\omega_B/\omega_R)^{1/3} > 10^3$, cf. Luo & Melrose 1992].

Due to the lower γ required for TIME, it is plausible that the radiating particles can be identified as those of the pair plasma. However, one must require that the distribution function has the characteristics of an effective population inversion, that is, $\partial f/\partial \gamma > 0$ at a value of γ that satisfies equation (19). In the polar cap models – e.g. Ruderman & Sutherland (1975) and Arons (1981) – a primary beam is accelerated in the gap and the primary beam particles radiate high-energy photons which in turn produce electron–positron pairs. Therefore the pulsar magnetosphere consists of a dense pair plasma and energetic beams (of electrons or positrons or ions). In Arons' (1981) model, the lower cut-off of the pair-plasma distribution is ≥ 10 . In this case the radiating particles that are capable of amplifying waves are those on the positive slope at the lower energy end of the distribution $f(\gamma)$, provided that the spread of momenta in the stable region $df(\gamma)/d\gamma < 0$ is not too large.

Once the condition (19) is satisfied, maser emission can occur for any $\alpha \neq 0$, but maser emission is important only when α exceeds an appropriate minimum value. This follows by estimating the maximum modulus of the optical depth for negative absorption:

$$\tau_a \approx 2 \left(\frac{\omega_p}{\omega_R} \right)^2 \left(\frac{\omega_R}{\omega} \right)^{8/3} \alpha^2. \quad (20)$$

As an example, for $R_B = 1.5 \times 10^5$ m (cf. Tables 1a–c), $\omega = 10^8$ s $^{-1}$, $N_0 = 5 \times 10^{21}$ m $^{-3}$ and $\alpha = 0.1$ (cf. Tables 1a–c), one would have $\tau_a \approx 4 \times 10^2$. In deriving (20), one takes the minimum Lorentz factor $\gamma \approx (\omega/\omega_R)^{1/3}$. The optical depth decreases rapidly as γ increases, $\tau_a \propto 1/\gamma^4$. From equation (20), the condition $\tau_a > 1$ requires

$$\alpha > (1/\sqrt{2})(\omega_R/\omega_p)(\omega/\omega_R)^{4/3}. \quad (21)$$

Thus, for the parameters used above, the ratio of the curvature radius to torsion radius should be no less than 10^{-3} . Here the minimum α is derived using the smallest Lorentz factor given by the right-hand side of the inequality (19). Thus a relatively larger α is required to obtain an efficient amplification.

The results presented in Figs 2 and 3 can be readily generalized to the case where radiating particles have a dis-

Table 1. (a) The radii of curvature and torsion. The ratio of the quadrupole to the dipole fields is assumed to be $n^{(q)} = 4$. The field line ends at the light cylinder $\Phi = 0.2$, $\Theta = \pi/2$.

ρ/ρ_0	Θ	Φ	R_T/ρ_0	R_B/ρ_0
10 ²	0.169	0.170	7.987 × 10 ⁴	7.44 × 10 ²
50	0.146	0.134	2.356 × 10 ⁴	4.04 × 10 ²
20	0.167	0.068	8.311 × 10 ³	1.32 × 10 ²
10	0.237	0.029	7.031 × 10 ³	52.9
5	0.350	0.011	2.494 × 10 ⁴	26.5
3	0.434	0.00556	4.898 × 10 ³	19.49
2	0.487	0.00349	1.593 × 10 ³	16.85
1.5	0.518	0.00261	1.084 × 10 ³	15.79

Table 1. (b) The radii of curvature and torsion. The field line ends at the light cylinder $\Phi = \pi/3$ and $\Theta = \pi/2$.

ρ/ρ_0	Θ	Φ	R_T/ρ_0	R_B/ρ_0
10 ²	0.158	0.904	2.133 × 10 ⁴	8.18 × 10 ²
50	0.150	0.580	5.947 × 10 ³	4.06 × 10 ²
20	0.176	0.266	2.141 × 10 ³	1.29 × 10 ²
10	0.244	0.115	1.768 × 10 ³	52.17
5	0.353	0.044	6.069 × 10 ³	26.41
3	0.434	0.023	1.181 × 10 ³	19.49
2	0.486	0.014	4.145 × 10 ²	16.88
1.5	0.516	0.011	2.222 × 10 ²	15.84

Table 1. (c) The radii of curvature and torsion. The field line ends at the light cylinder $\Phi = \pi/2$ and $\Theta = \pi/2$.

ρ/ρ_0	Θ	Φ	R_T/ρ_0	R_B/ρ_0
10 ²	0.159	0.973	2.124 × 10 ³	8.17 × 10 ²
50	0.152	0.600	5.802 × 10 ³	4.02 × 10 ²
20	0.178	0.275	2.071 × 10 ³	1.28 × 10 ²
10	0.246	0.118	1.720 × 10 ³	52.00
5	0.355	0.045	5.806 × 10 ³	26.30
3	0.436	0.023	1.203 × 10 ³	19.44
2	0.488	0.015	3.937 × 10 ²	16.83
1.5	0.519	0.011	2.287 × 10 ²	15.76
1.1	0.547	0.008	1.402 × 10 ²	15.07

tribution with a spread in Lorentz factors. Let $\Gamma(\gamma, \theta)$ be the absorption coefficient for a given Lorentz factor γ . As shown in Figs 2 and 3, $\Gamma(\gamma, \theta_0)$ is negative at $\theta_0 \leq 10^{-4}$ for γ between 50 and 5×10^2 . For $\gamma > 500$, numerical calculations show that $\Gamma(\gamma, \theta_0)$ is negligibly small. Thus one can show that the net negative absorption at θ_0 can be obtained after integrating $\Gamma(\gamma, \theta_0)$ over the distribution $f(\gamma)$, provided that particles with energy in the region $df(\gamma)/d\gamma > 0$ contribute most to the integration (16). As an example, we consider the distribution $f(\gamma) \propto \gamma^{-1.5} \exp(-\gamma_0/\gamma)$ (Arons 1981) with the peak at $\gamma_0 = 100$. The distribution is assumed to be in the region $30 \leq \gamma \leq 10^3$. By numerically integrating (16) over $f(\gamma)$, one has $\langle \Gamma \rangle / (\omega_R \langle \gamma \rangle) \approx -35$ at $\theta \approx 6 \times 10^{-3} / \langle \gamma \rangle$ (where $\langle \dots \rangle$ represents averaging over the relevant distribution).

4.2 Non-dipole field

A non-dipole field structure can occur either close to the star's surface or near the light cylinder. Consider the first field line distortion near the light cylinder where the rotation

causes the field lines to sweep back (Shitov 1983). The spin-down of a neutron star can be attributed to a net Polytning flux being carried away from the system. There is necessarily a toroidal wave term B_t comparable to the dipole contribution to \mathbf{B} near the light cylinder associated with the field lines being swept back. Let us assume that the dipole field line is locally circular (in an azimuthal plane that contains the dipole axis) and that the field line deviates into the normal direction to this plane due to the presence of B_t . The resultant field line is twisted with $\alpha \approx B_t/B$, where B is the dipole field. Thus field line torsion due to rotational sweep-back may result in maser emission provided that the particle motion is approximately one-dimensional.

The non-dipole field structure near the stellar surface is attributed to higher multipole components. To see how the multipole modification gives rise to field line twisting, consider the multipole expansion for the magnetic field of the star,

$$\mathbf{B} = \mathbf{B}^{(d)} + \mathbf{B}^{(q)} + \dots, \quad (22)$$

where $\mathbf{B}^{(d)}$ and $\mathbf{B}^{(q)}$ are the dipole and the quadrupole fields, respectively. For each multipole field one may define a multipole axis, such that, for Cartesian axes with one axis oriented along the multipole axis, the tensor that describes the multipole is diagonalized. In general, in equation (22) the dipole, quadrupole and other axes are different and are different from the rotation axis. A twisted field is implied when the dipole and quadrupole axes are different.

To estimate α , we consider the field configuration as a result of superposition of a dipole and a quadrupole with two axes at an angle $\Delta\Theta_0$. For the dipole, in spherical polar coordinates (ρ, Θ, Φ) (with the polar axis along the dipole axis) the magnetic field can be written

$$B_\rho^{(d)} = B_0 \left(\frac{\rho_0}{\rho} \right)^3 \cos \Theta, \quad (23a)$$

$$B_\Theta^{(d)} = \frac{1}{2} B_0 \left(\frac{\rho_0}{\rho} \right)^3 \sin \Theta, \quad (23b)$$

where B_0 and ρ_0 represent the dipole field at the star's surface (at $\rho = \rho_0$, $\Theta = 0$) and the radius of the star, respectively. The quadrupole field can be written in its own coordinate system (ρ, Θ', Φ') as

$$B_\rho^{(q)} = \frac{1}{2} n^{(q)} B_0 \left(\frac{\rho_0}{\rho} \right)^4 (3 \cos^2 \Theta' - 1), \quad (24a)$$

$$B_\Theta^{(q)} = n^{(q)} B_0 \left(\frac{\rho_0}{\rho} \right)^4 \cos \Theta' \sin \Theta', \quad (24b)$$

where the quadrupole field at the star's surface (at $\rho = \rho_0$, $\Theta' = 0$) is given by $n^{(q)} B_0$. Using (B7), the quadrupole field can be re-expressed in terms of the dipole coordinates, i.e.

$$B_\rho^{(q)} = B_\rho^{(q)}(\rho, \Theta, \Phi), \quad (25a)$$

$$B_\Theta^{(q)} = B_\Theta^{(q)}(\rho, \Theta, \Phi) \cos \zeta, \quad (25b)$$

$$B_\Phi^{(q)} = B_\Phi^{(q)}(\rho, \Theta, \Phi) \sin \zeta, \quad (25c)$$

where the angle ζ is defined by (cf. Appendix B)

$$\tan \zeta = \frac{\sin \Delta\Theta_0 \sin \Phi}{\cos \Delta\Theta_0 \sin \Theta - \sin \Delta\Theta_0 \cos \Theta \cos \Phi}, \quad (26)$$

and $B_\rho^{(q)}(\rho, \Theta, \Phi)$, $B_\Theta^{(q)}(\rho, \Theta, \Phi)$ are derived from equations (24a) and (24b) using (B7). The two axes pass through the centre of the star (cf. Fig. 4a). The field line twisting must occur in regions where the planar field lines of a dipole field are complemented by the azimuthal component $B_\Phi^{(q)}$ of the field from the quadrupole. From equations (25a)–(25c), the condition for field line twisting is $\Delta\Theta_0 \neq 0$ and $\Phi \neq 0$, where we assume $\Delta\Theta_0 < \pi/2$. The non-dipole field line configuration is symmetric about the plane $\Phi = 0$ (i.e. the plane defined by the two polar axes \mathbf{P}_d and \mathbf{P}_q as shown in Fig. 4a). The field lines at either sides of the plane are twisted. Unlike a pure dipole field, in which the field line structures at the two poles are symmetric, the modified polar field in one hemisphere is different from that in the other hemisphere.

Evaluation of the radii of torsion and curvature at each point of a field line involves the solution of the differential equations for the field line. Let $B_\rho = B_\rho^{(d)} + B_\rho^{(q)}$, $B_\Theta = B_\Theta^{(d)} + B_\Theta^{(q)}$ and $B_\Phi = B_\Phi^{(q)}$. The magnetic field lines are now described by the following differential equations:

$$\frac{d\rho}{B_\rho} = \frac{\rho d\Theta}{B_\Theta} = \frac{\rho \sin \Theta d\Phi}{B_\Phi}. \quad (27)$$

The radii of curvature and torsion are defined by equations (B1) and (B2), respectively. One may numerically calculate R_B and R_τ using equations (B1)–(B4) and (27). Consider a field line from the star to the point p_L : $\rho = c/2\pi\Omega$, $\Theta = \pi/2$, $\Phi \neq 0$, where Ω is the angular velocity of the star. The spherical coordinates of any point along this field line can be obtained by integrating (27) from p_L to the point considered. Given the position in terms of the spherical coordinates, one can calculate R_τ and R_B . Tables 1(a)–(c) list R_τ and R_B obtained at different radii ρ , which together with angles Φ and Θ are the numerical solution of the differential equation (27). The differential equations are solved using the fourth-order Runge–Kutta scheme with adaptive step size. We assume that the two poles have an angle $\Delta\Theta_0 = \pi/4$, and that the pulsar period is $P = 1$ s. From the table one can see that, due to the quadrupole, the region where the open field line flux tube intersects the star's surface is shifted approximately 31° (for $\Delta\Theta_0 = \pi/4$) towards the quadrupole axis \mathbf{P}_q . The field line is severely twisted at a distance of a few stellar radii. From Table 1(c), one has $\alpha \approx 0.1$ near the star. The ratio of curvature radius to torsion radius is large enough to give rise to curvature maser emission [i.e. the condition (21) can be satisfied]. The quadrupole component decreases rapidly as the radial distance increases. At distances $\rho > 10^2 \rho_0$ the dipole component is dominant and torsion can be neglected. Thus the relevant maser emission (TIME) can only occur at a small radial distance.

4.3 Pulse structure due to field complexity

In this section, we restrict the discussion to field line distortion near the star's surface, and discuss possible observational consequences of such a field complexity. As shown in the previous sections, effective amplification requires that the particle density be high. This condition can easily be satisfied near the stellar surface, and radio emission can occur provided that the ratio of the radius of curvature to the radius of torsion is large enough ($\alpha \gg 10^{-3}$).

The pulse structure is determined by the geometry of field line flux tubes in the emission region, as the radiation is prac-

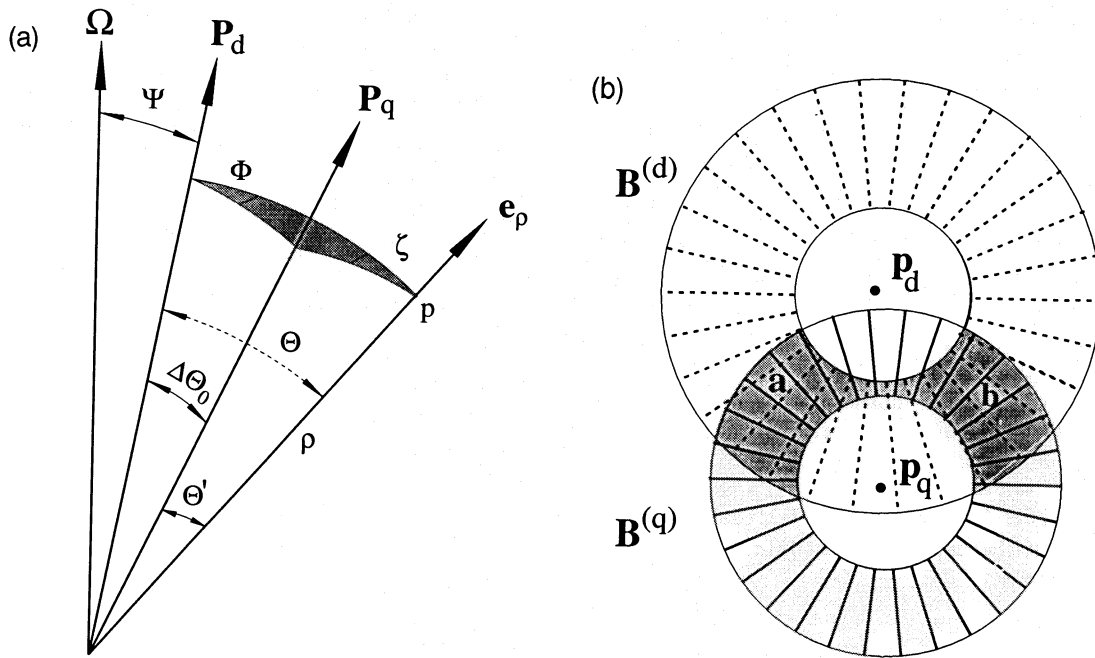


Figure 4. A field configuration consisting of a dipole and a quadrupole. (a) Their polar axes are represented by P_d and P_q , respectively. The polar axes, which are assumed to pass through the star's centre, are at an angle $\Delta\Theta_0$ to each other. The angular velocity is Ω , and the inclination angle is Ψ . (b) A down-to-pole view of the field line geometry. The dotted and solid radial lines represent, respectively, the magnetic field of the isolated dipole and quadrupole projected on to the sky. The total magnetic field is the combination of the dipole and quadrupole. The field line twisting can occur in the overlap part where $B_\theta^{(d)}$ is perpendicular to $B_\theta^{(q)}$.

tically along the field line direction. When the field line complexity is attributed to a quadrupolar term, the open field line cones at two modified poles are not identical. Let us consider the open field line cone within which the dipole and the quadrupole have the same polarity. As shown in the previous section, there is a plane that contains the dipole and quadrupole axes (P_d and P_q as shown in Fig. 4a). In this plane the field lines are planar. Field lines on both sides of this plane are twisted, forming two twisted flux tubes (we also call them twisted cones). The torsion-induced maser emission occurs in these two twisted flux tubes. At large radial distances, the dipole dominates and the two twisted flux tubes become a single dipole cone within which field lines are approximately planar. When the line of sight passes across the plane of symmetry, emission regions are encountered on both sides, but there is no emission in the plane itself. If the radiation from each side is encountered in two well-separated cones, then a double-peaked profile is observed. We have yet to explore the geometry in detail, to plot the allowed ranges of angular separation of the double-peaked profiles, and to determine whether these can merge into an unresolved single peak.

The observed pulse width is in general related to the opening angle of the divergent field lines in the emission region. One may obtain the opening angle by estimating the radial dependence of the cross-sectional area of the twisted (open field line) cones. Near the star the cross-sectional shape of each twisted cone is approximately a half-ellipse with one semi-axis Δx in the plane of symmetry (the whole open field line cone gives a cross-section of elliptical shape; e.g. Barnard & Arons 1982). The other semi-axis is normal to the plane and is given approximately by $\Delta y = \rho \sin \Theta \sin \Phi$. Thus the

opening angle in the plane perpendicular to the polar plane is $\Delta\Theta_y \approx \Theta \Phi$, where Θ and Φ can be expressed as functions of ρ . From the numerical solution in Table 1, the angle $\Delta\Theta_y$ at the surface $\rho = \rho_0$ is smaller than in the dipole case. As ρ increases, the angle increases more rapidly than for the dipole. For example, in Table 1(c), at $\rho = 10\rho_0$, one has $\Delta\Theta_y \approx 2^\circ$. Thus one expects a stronger radial dependence of the pulse width than in the dipole case. Closely analogous to the work by Barnard & Arons (1982), one may estimate the opening angle $\Delta\Theta_x$ in the P_d - P_q plane. This angular width is determined by Δx , which can be derived from Δy using flux conservation, as, for example, in Barnard & Arons (1982). This angle is estimated to be $\Delta\Theta_x = 2(\rho_0/\rho_L)[B_0/B(\rho)](\rho_0/\rho)^2/(\Theta \Phi)$, where ρ_L is the radius of the light cylinder. For $n^{(q)} = 4$, $P = 1$ s, the angular width can be as large as a few degrees.

When the emission is from the other pole, where P_d and P_q have opposite polarities, one may observe pulses with two widely separated components (looking like 'interpulses'). The separation between two components can be as large as 180° in longitude. Hence this mechanism can provide an alternative explanation for high-frequency pulses with two interpulse-like components.

Another distinct feature associated with surface field complexity is that the polarization position angle variation is relatively small. In a strictly dipole field line geometry, the position angle can sweep through a large angular range ($\geq 180^\circ$). In the torsion-induced maser emission the polarization is in the direction perpendicular to the field line osculating plane (i.e. the polarization is approximately in the binormal direction of the field line). As shown in Fig. 4(b), the variation of the binormals of the field lines within the

twisted cones through regions a and b is less than 90° . Thus one expects the variation of polarization position angle to be small (cf. Barnard & Arons 1982).

5 SATURATION OF MASER EMISSION

There are three effects that may lead to reduction in the growth rate: (i) quasi-linear diffusion; (ii) ponderomotive force effects; and (iii) field line geometric effect. It is shown below that the most effective mechanism for maser saturation is that due to the quasi-linear diffusion. The field line geometric effect can be important only when the field lines are severely twisted.

Induced processes cause quasi-linear diffusion, which involves diffusion in momentum space that causes the distribution function to evolve so as to reduce the growth rate. This may lead to saturation of the maser. Parallel diffusion, which is the only relevant diffusion in the one-dimensional case, may be described by a parallel diffusion coefficient (Melrose 1980)

$$D_{\varphi\varphi} = \int d\omega (\hbar k_\varphi)^2 \left[\frac{\eta(\omega, \theta_0)}{\hbar\omega} \right] N(\mathbf{k}) \Delta\Omega, \quad (28)$$

where $\Delta\Omega$ is the solid angle subtended by the radiation beam pattern, $\eta(\omega, \theta_0)$ is the curvature spectral power at the angle θ_0 and $N(\mathbf{k})$ is the photon occupation number. We assume that the negative absorption peak is at θ_0 . Let $\Delta t_d = p_\varphi^2 / D_{\varphi\varphi}$ be the time-scale for the diffusion. Using the approximation $\hbar k_\varphi \approx \hbar k$ and equation (28), and assuming that the curvature radiation frequency is ω_0 , one has

$$\Delta t_d \approx \frac{1}{(2\pi)^3} \left(\frac{\omega_0^3}{c^3 N_0} \right) \left[\frac{m\gamma c^2}{\omega_0 \eta(\omega_0, \theta_0)} \right] R_{wp}^{-1}, \quad (29)$$

where R_{wp} is the ratio of wave energy density to particle energy density. One can estimate the upper limit of R_{wp} by comparing the diffusion time-scale with the emission time-scale $\Delta t_e \approx R_B / c\gamma$. With the same choice of parameters as in Figs 2 and 3, using $\omega_0 \eta(\omega_0, \theta_0) \approx \omega_0 \eta(\omega_0, 0) \approx (5/32\pi)(q^2 c / 4\pi\epsilon_0 R_B^2) \gamma^7 (\alpha/2\gamma^2)^2$, one has the saturated wave energy level $R_{wp} \sim 10^{-4}$. Thus the upper limit to the brightness temperature can be as high as 10^{32} K.

Since wave amplification occurs within a relatively small length-scale, one expects to have a large spatial gradient in the wave field. Due to this gradient, there is a force (called ponderomotive force) on the particles. As a consequence of the ponderomotive effect, the particles with relatively small Lorentz factors are expelled from the emission region. Let E_0 be the initial electric field perturbation. Then, for distance $l_e = c\Delta t_e = R_B/\gamma$, the wave energy level after being amplified by e^τ is W_w . The ponderomotive force is proportional to the gradient of the wave energy density which is

$$dW_w/dl \approx 2\tau W_w/l_e, \quad (30)$$

where l is a distance along the field line from the star's surface. Similar to the discussion by Melrose (1978), the time-scale for the dispersal of the particles with lower energy by the ponderomotive force is

$$\Delta t_d \approx \frac{1}{(2\tau)^{1/2}} \left(\frac{\gamma l_e}{c} \right) \left(\frac{W_p}{W_w} \right)^{1/2}. \quad (31)$$

Therefore one has

$$\frac{\Delta t_d}{\Delta t_e} = \frac{\gamma}{(2\tau R_{wp})^{1/2}}. \quad (32)$$

The dispersal is unimportant only for $\Delta t_d/\Delta t_e \gg 1$, which requires

$$\tau \ll \frac{\gamma^2}{2R_{wp}}. \quad (33)$$

The upper limit on the optical depth increases as γ increases, since, for increasing τ , the ponderomotive effect becomes less important. If one takes the smallest Lorentz factor implied by equation (19), $\gamma = (\omega/\omega_R)^{1/3}$, and assumes $R_{wp} = 1$, one has $\tau \ll (\omega/\omega_R)^2/2$. This upper limit is much less stringent than that due to quasi-linear diffusion. Therefore, quasi-linear diffusion is the more effective in determining maser saturation.

The length-scale available for wave amplification can also be constrained by the field line geometry itself. A particle initially moving along the field line can subsequently acquire an angle with respect to the *initial* osculating plane, since the osculating plane of a twisted field line changes along the field line. This angle is given approximately by

$$\delta\theta \approx \frac{1}{2} \left(\frac{\Delta l}{R_B} \right)^2 |\tan \alpha|, \quad (34)$$

where Δl is the distance that a particle propagates along the field line. Wave amplification requires that the angle defined in equation (34) be smaller than θ_0 , the angular location of the negative absorption peak. Hence, given a field geometry, e.g. R_B , α , etc., one has the e-folding time $\Delta t_a = \Delta l/c = 2|\theta_0/\tan \alpha|^{1/2}/\omega_R$. For sufficiently large $\tan \alpha > 4\theta_0\gamma^2 \approx 1$ (with the Lorentz factor $\gamma = 50$ and $\theta_0 \approx 10^{-4}$), the time-scale Δt_a can be smaller than the emission time-scale $\Delta t_e = R_B/\gamma c$ and the radiation level is limited by the effective optical depth $\tau_{\text{eff}} = \tau_a \Delta t_a / \Delta t_e < \tau_a$, with τ_a given by equation (20).

6 CONCLUSIONS

In this paper the field line geometrical effect on curvature emission and absorption is investigated in detail, and its implications for pulsar radio emission are discussed. The main results are summarized as follows.

(1) Maser emission can occur for plasma streaming along twisted field lines. For torsion-induced maser emission, the amplified waves are transverse, with polarization approximately perpendicular to the field line (osculating) plane. Thus the mechanism can produce only linear polarization. To explain circular polarization as observed in some pulsars one needs some mechanism that can convert linear polarization into circular polarization. One possible way of such a conversion is to take into account of the birefringent effect of the magnetized pair plasma (Melrose 1979).

(2) The properties required of the radiating particles are (i) an inverted energy spectrum (equation 7a), (ii) modest Lorentz factors $\gamma \approx 37$ –50, and (iii) that the contributions of electrons and positrons have the same sign (unlike the case of curvature-drift-induced maser emission, where positrons

and electrons contribute with opposite sign to the growth rate).

(3) Maser emission occurs approximately in the field line direction. The intrinsic angular width is less than 0.1° . The observed angular width should be related to the opening angle of the bunch of field lines in the emission region, which is larger than the intrinsic angular width.

(4) Torsion-induced maser emission gives rise to a distinct polarization feature where the position angle variation is relatively small compared with the pure dipole case (Barnard & Arons 1982). Since for the majority of pulsars there is a position angle swing of the linear polarization, this feature can help to identify those pulsars in which field line complexity is relevant to radio emission.

(5) This mechanism can produce either a pulse with two components, like ‘interpulses’, or a double-peaked single pulse. If the emission originates from a non-dipole, open field line region where the merged field lines are due to a dipole and a quadrupole with opposite polarities, one sees a pulse with two widely separated components as ‘interpulses’, since the open field lines in this region form two separated cones ending diametrically at two neighbouring poles of the quadrupole field on the star. If the emission originates from an open field line region that is due to a dipole and a quadrupole with the same polarities, one sees a single pulse with two peaks. With decreasing radial distance, the two peaks become smaller.

(6) Maser emission can be saturated due to quasi-linear diffusion. The ponderomotive effect may result in reduction of the growth rate by expelling the lower energy particles from the emission region; however, it is not as effective as quasi-linear diffusion. Field line geometry can also limit the growth rate when the field line torsion is sufficiently large. The more severely twisted the field lines, the shorter the e-folding time available for wave amplification. The lowest ratio of the curvature to torsion radii above which the geometrical constraint on the growth rate becomes important is estimated to be $R_B/R_\tau > 4\theta\gamma^2 \approx 1$.

ACKNOWLEDGMENTS

We thank Mark Walker for helpful comments.

REFERENCES

- Arons J., 1981, in Sieber W., Wielebinski R., eds, Proc. IAU Symp. 95, Pulsars. Reidel, Dordrecht, p. 69
 Arons J., Barnard J., 1986, ApJ, 302, 120
 Barnard J., Arons J., 1982, ApJ, 254, 713
 Barnard J., Arons J., 1986, ApJ, 302, 138
 Blandford R. D., 1975, MNRAS, 170, 551
 Chandrasekhar S., 1960, Radiative Transfer. Dover, New York
 Jackson J. D., 1968, Classical Electromagnetic Field. Wiley, New York
 Krolik J. H., 1991, ApJ, 373, L69
 Kuz'min A. D., 1992, in Hankins T. H. et al., eds, Proc. IAU Colloq. 128, The Magnetospheric Structure and Emission Mechanism. Pedagogical Univ. Press, Zielona Gora, p. 2
 Lominadze Dzh. G., Machabeli G. Z., Melikidze G. I., Pataraya A. D., 1986, Sov. J. Plasma Phys., 12, 712
 Luo Q., 1993, Proc. Astron. Soc. Aust., 10, 258
 Luo Q., Melrose D. B., 1992, MNRAS, 258, 616
 Luo Q., Melrose D. B., Machabeli G. Z., 1994, MNRAS, 268, 159

- McCray R., 1966, Sci., 154, 1320
 Melrose D. B., 1978, ApJ, 225, 557
 Melrose D. B., 1979, Aust. J. Phys., 32, 61
 Melrose D. B., 1980, Plasma Astrophysics, Vol. 1. Gordon & Breach, New York
 Ruderman M. A., 1991, ApJ, 366, 261
 Ruderman M. A., Sutherland P. G., 1975, ApJ, 196, 51
 Rybicki G. B., 1984, in Kalkofen W., ed., Escape Probability Methods in Radiative Transfer. Cambridge Univ. Press, Cambridge, p. 21
 Shitov Yu. P., 1983, SvA, 27, 314
 Zheleznyakov V. V., 1967, Sov. Phys. JETP, 24, 381
 Zheleznyakov V. V., Suворov E. V., 1972, Ap&SS, 15, 24

APPENDIX A

In this appendix, the spectral power for a particle moving along a locally helical field line is derived from the synchrotron spectral power. The synchrotron spectral power is given by (Zheleznyakov & Suворov 1972; Melrose 1980)

$$\eta(\omega, \theta_k) = \frac{q^2 \omega^2}{24\pi^4 \epsilon_0 c n \omega_B (1 + T^2)} \times \left| \frac{\cos \theta_k - n\beta \cos \theta_p}{\sin \theta_k} T\xi^{-1} K_{1/3}(y) + n\beta \sin \theta_p \xi^{-2} K_{2/3}(y) \right|^2, \quad (\text{A1})$$

with

$$\bar{x} = \frac{n\beta \sin \theta_p \sin \theta_k}{1 - n\beta \cos \theta_p \cos \theta_k}, \quad (\text{A2})$$

$$\bar{y} = \frac{1}{\gamma(1 - n\beta \cos \theta_p \cos \theta_k)}, \quad (\text{A3})$$

$$\xi = \left[\frac{\bar{x}}{2(1 - \bar{x})} \right]^{1/2}, \quad (\text{A4})$$

$$y = \left(\frac{\omega}{3\omega_B} \right) \left(\frac{\bar{x}}{\bar{y}} \right) \xi^{-3}, \quad (\text{A5})$$

where θ_p is the pitch angle and where the wave vector \mathbf{k} is expressed in terms of polar angles θ_k and ϕ_k with respect to the magnetic field \mathbf{B} . To obtain the curvature spectral power, we define α as the angle between the field line and the plane on which field line projection is locally circular of radius R . We also define the angle between wave vector and field line by θ . Then the spectral power (equation 11) can be derived by substituting

$$\theta_p \rightarrow \frac{\pi}{2} - \alpha,$$

$$\theta_k \rightarrow \frac{\pi}{2} - \alpha - \theta$$

into equation (A1).

APPENDIX B

In this appendix, the explicit expressions for the radii of curvature and torsion of three-dimensional field lines are given. The radii of curvature and torsion can be conveniently defined in terms of the Cartesian coordinates (x, y, z) , with the z -axis along the dipole axis, as follows:

$$R_B = \frac{(x^2 + y^2 + z^2)^{3/2}}{[(\dot{y}\ddot{z} - \dot{z}\ddot{y})^2 + (\dot{z}\ddot{x} - \dot{x}\ddot{z})^2 + (\dot{x}\ddot{y} - \dot{y}\ddot{x})^2]^{1/2}}, \quad (\text{B1})$$

$$R_\tau = \frac{1}{|\mathbf{G}|} [(\dot{y}\ddot{z} - \dot{z}\ddot{y})^2 + (\dot{z}\ddot{x} - \dot{x}\ddot{z})^2 + (\dot{x}\ddot{y} - \dot{y}\ddot{x})^2], \quad (\text{B2})$$

$$\mathbf{G} = \begin{vmatrix} \dot{x} & \dot{y} & \dot{z} \\ \ddot{x} & \ddot{y} & \ddot{z} \\ \dddot{x} & \dddot{y} & \dddot{z} \end{vmatrix}, \quad (\text{B3})$$

where $\dot{x} = dx(\nu)/d\nu$, $\ddot{x} = d^2x(\nu)/d\nu^2$ and $\dddot{x} = d^3x(\nu)/d\nu^3$ with parametrization $x = x(\nu)$. On transforming to spherical co-

ordinates (ρ, Θ, Φ) ,

$$\begin{aligned} x &= \rho \sin \Theta \cos \Phi, \\ y &= \rho \sin \Theta \sin \Phi, \\ z &= \rho \cos \Theta, \end{aligned} \quad (\text{B4})$$

one can write all relevant derivatives of $x(\nu)$, $y(\nu)$ and $z(\nu)$ in terms of spherical coordinates. In the numerical calculation of R_B and R_τ we choose the parametrization $\nu = \Theta$.

The angle ζ in equations (25b) and (25c) can be derived from the following relation:

$$\frac{\sin \Delta\Theta_0}{\sin \zeta} = \frac{\sin \Theta'}{\sin \Phi}, \quad (\text{B5})$$

where all angles are defined in Fig. 4. Using (B5) and the relations

$$\cos \Delta\Theta_0 = \cos \Theta' \cos \Theta + \sin \Theta' \sin \Theta \cos \zeta, \quad (\text{B6})$$

$$\cos \Theta' = \cos \Delta\Theta_0 \cos \Theta + \sin \Delta\Theta_0 \sin \Theta \cos \Phi, \quad (\text{B7})$$

one can obtain equation (26).